High-velocity impact response of 3D-printed composite mechanical metamaterials

International Journal of Mechanical Sciences 286 (2025) 109905

Contents lists available at ScienceDirect

International Journal of Mechanical Sciences

journal homepage: www.elsevier.com/locate/ijmecsci

High-velocity impact response of 3D-printed composite mechanical metamaterials

Tom Fisher [a],*, Zafer Kazancı [a], José Humberto S. Almeida Jr. [b]

[a] Advanced Composites Research Group, School of Mechanical and Aerospace Engineering, Queen's University Belfast, Belfast, BT9 5AH, UK
[b] Department of Mechanical Engineering, LUT University, Lappeenranta, Finland

ARTICLE INFO

Keywords:
3D-printing
High-velocity impact
Composite
Metamaterials
Hybrid structures
Parametric analysis

ABSTRACT

This study explores the high-velocity impact response of 3D-printed composite mechanical metamaterials through a combination of experimental testing and numerical simulations. Auxetic structures demonstrated a marked reduction in transmitted force and an extended force duration, both of which are advantageous for mitigating impact-related injuries. Specifically, the double arrowhead auxetic geometry reduced the transmitted force by 44% compared to conventional hexagonal structures, albeit at the cost of 17% greater deformation. Novel hybrid designs, integrating auxetic and conventional geometries, achieved a decoupled control of deformation and force responses. For instance, a re-entrant auxetic structure on the impact face, transitioning into a hexagonal configuration, led to a 10% increase in deformation compared to the reverse orientation while maintaining a similar transmitted force. Additionally, a comprehensive parametric study was conducted to examine the influence of cell size and relative density on the overall impact performance of these metamaterials.

1. Introduction

Cellular structures are widely studied due to their high energy absorption and lightweight properties [1–5], making them ideal for applications such as blast protection and impact mitigation. These structures absorb energy through plastic bending and buckling of cell walls, enabling increased energy absorption and a reduced peak force compared to the base material [6]. Recent advancements in additive manufacturing allow for the fabrication of complex cellular structures with tailored mechanical properties [3,4] via, for example, stereolithography (SLA) [7–11], fused filament fabrication (FFF) [12–16] and selective laser melting (SLM) [17–20]. This has led to significant progress in fields where energy absorption is critical, such as automotive crashworthiness [21–25] and blast protection [26,27]. In particular auxetic structures, which exhibit a negative Poisson's ratio, have shown superior performance under blast and impact loading compared to non-auxetic counterparts [28,29].

Previous studies have explored the energy absorption capabilities of various 3D-printed auxetic structures [30–35]. Zhang et al. [36] developed a novel auxetic unit cell inspired by a windmill, an extension of the anti-tetra-missing rib structure. This structure maintained a negative Poisson's ratio over a larger strain rate than the original, improving the energy absorption capacity during quasi-static compression. A study by Linforth et al. [34] considered the energy absorption of aluminium laser cut with an auxetic oval pattern via both quasi-static and dynamic experiments finding no significant difference. Novak et al. [37], however, found a major increase in specific energy absorption of chiral auxetic structures at high strain rates. Najafi et al. [38] compared the energy absorption capabilities of re-entrant, arrowhead, and anti-tetrachiral structures under quasi-static and low-velocity impact conditions. They found that the anti-tetrachiral and arrowhead geometries outperformed the re-entrant design in quasi-static tests, but the performance converged under low-velocity impacts. This sensitivity to loading conditions highlights the importance of understanding the impact response at high velocities. Qi et al. [39] numerically investigated the ballistic resistance of standard and auxetic (re-entrant) aluminium honeycomb sandwich panels, finding the auxetic structure gave the best ballistic performance, a result echoed by Mohamed et al. [40]. Madke & Chowdhury [41] investigated the impact performance of auxetic sandwich structures with braided face sheets and 3D re-entrant cores. They found that for an impact velocity of 211.8 m/s, and near-equal mass, sandwich structures with a 3D re-entrant core had a significantly higher energy absorption than the non-auxetic counterpart. Critchley et al. [42] showed that additively manufactured auxetic

* Corresponding author.
E-mail addresses: tfisher05@qub.ac.uk (T. Fisher), z.kazanci@qub.ac.uk (Z. Kazancı), humberto.almeida@lut.fi (J.H.S. Almeida Jr.).

https://doi.org/10.1016/j.ijmecsci.2024.109905
Received 21 August 2024; Received in revised form 11 November 2024; Accepted 15 December 2024
Available online 24 December 2024

honeycombs mitigated blast impulse and reduced peak transmitted pressure compared to traditional honeycombs. They noted that there is a need for future studies to investigate the effect of geometric parameters and relative density as well as explore alternative geometries such as arrowhead structures. These gaps have been addressed in this work. A recent review on the impact performance of auxetic structures [43] recommended the investigation of hybrid structures, that is cellular structures containing more than one type of geometry, which has been explored in this work. Previous studies have explored different types of hybrid structures for example combining two unit cells into one [44–48], alternating cell geometry between layers [49–51] and grading the thickness throughout the structure [52–54]. Tan et al. [48] designed a hierarchical structure consisting of re-entrant cells with honeycomb or triangular substructures in place of the cell walls. They found that the introduction of hierarchy into sandwich panels significantly reduced the peak force during crushing and improved the impact resistance. Combining auxetic and non-auxetic geometries into one unit cell, for example AuxHex [47], has been shown to enhance energy absorption properties compared to a standard auxetic re-entrant structure. Angle gradient honeycombs, where the angle changes throughout the structure [55–58], have been shown to enhance control of the global and local mechanical response [55] and improve energy absorption compared to other gradient structures [57].

Building on previous studies, this work investigates the high-velo city impact response of 3D-printed composite mechanical metamaterials through both experimental validation and extensive numerical simulations. Despite significant research on auxetic structures, there remains a need to fully understand the dynamic response of these structures under high-velocity impacts. This study addresses this gap by examining the performance of 3D-printed composite cellular structures through a combination of experimental testing and finite element simulations. A key contribution of this paper is the comprehensive parametric study which investigates the effects of cell geometry, size, and relative density on the impact performance of these structures. By focusing on how these parameters affect force transmission and deformation, the study provides new insights that can inform the optimisation of cellular structures for impact mitigation. Three main geometries are considered: hexagonal [59–61], and two auxetic structures — re-entrant [62,63] and double arrowhead [64–66]. Additionally, this work explores hybrid structures, combining auxetic and conventional geometries. These hybrid configurations demonstrate promising potential for enhancing both force transmission and deformation control under high-velocity impacts, offering a new avenue for future research.

The remainder of this paper is organised as follows. Section 2 details the materials and methods used for both the experimental and numerical investigations, including the 3D-printed auxetic re-entrant structure and the impact testing setup. Section 3 presents and discusses the results, starting with the comparison between experimental and numerical findings, followed by an extended numerical analysis that includes ballistic impacts and parametric studies of relative density and cell size. Finally, Section 4 concludes the paper by summarising the key findings and suggesting avenues for future research.

2. Materials & Methods

This section details the experimental and numerical methods employed to investigate the impact response of 3D-printed composite structures. The primary objective of the experimental phase was to validate the numerical model by testing a 3D-printed auxetic re-entrant structure, which was impacted by a steel ball launched pneumatically. A numerical model was then developed to conduct parametric studies on the structure, investigating the effects of varying relative density and cell size on impact performance. The materials used, the experimental setup, and the modelling techniques are described next in detail.

2.1. Experimental

The experimental study was carried out at Simpact Engineering Ltd, Leamington Spa, England to assess the performance of a 3D-printed auxetic re-entrant structure under high-velocity impact. This experiment aimed to observe the deformation behaviour and force transmission characteristics of the structure when subjected to impact, thus providing a benchmark for the numerical simulations. The impact was conducted using a pneumatic launcher, and high-speed cameras were employed to capture the deformation process in real-time.

A $150 \times 150 \times 40$ mm cellular core consisting of a 4×10 array of re-entrant unit cells, Fig. 1, was 3D-printed by FFF with a 0.4 mm diameter nozzle [67,68] using the Markforged Mark Two printer. The structure had a 0.7 mm wall thickness, labelled "t". The structure was printed in the z direction with a layer height of 0.2 mm. The material used in this investigation was "Onyx", nylon reinforced with ≈13 wt% [69] short carbon fibres approximately 98 μm in length (full microstructure characterisation of "Onyx" is in [69]), which has been characterised in previous work [70]. The constitutive material models used in this work have been calibrated and validated for use in impact loading simulations in [71]. Face sheets 2 mm thick made of aluminium 6082-T6 (AA6082-T6) were bonded to the front and back of the printed structure using 3M DP460 epoxy adhesive.

The testing was carried out using a bespoke pneumatic launcher "SPL 6000" shown in Fig. 2(a). The projectile used was a 250 g hardened steel ball with a 40 mm diameter. The sample was positioned on a rigid base with the central 70 mm span supported from behind by a wooden block, as shown in Fig. 2(b). A pressure of 6 bar was used to launch the projectile at a velocity of 38 m/s towards the sample. A Photron FASTCAM SA1.1 675K-C2 high-speed camera was positioned above the sample, which was illuminated using three ICARUS LED lights, to capture the impact. The camera was set to record at a framerate of 12,000 fps using a shutter speed of 1/frame s. Post-processing of the camera footage, including calibration and motion tracking, was carried out using Photron FASTCAM Viewer 4 software.

2.2. Numerical modelling

A numerical model of the experimental setup was created using Abaqus 2020 FE platform, Fig. 3(a). The primary objective of the numerical simulations was to replicate the experimental results, providing a foundation for extending the analysis to higher velocity impacts and parametric studies. A Johnson–Cook material model, Table 1, was implemented for the 3D-printed core [70,71] with S4R [72–74] elements and the face sheet [75] with C3D8R elements. Damage for the 3D printed core was modelled using the ductile damage parameter pairs: rate (r, s^{-1}) and plastic strain (e), also given in Table 1. The projectile, base and rear support were modelled as analytical rigid parts. Hard contacts with a penalty friction of 0.3 [76–78] were applied to the whole model and a tie constraint was used to represent the bond between the printed part and the face sheets. The base and rear support were fixed ("encastre"), the core/face sheet assembly was free to move and the projectile was given an initial velocity of 38 m/s. No mass scaling was used in the numerical model to ensure the accuracy of the dynamic response.

The numerical model of the experimental impact was extended to explore ballistic impacts. A Kevlar face sheet is used to represent the materials used in body armour [79,80] and combat helmets [81,82]. Fig. 3(b) shows a 3D-printed structure with dimensions of $130 \times 130 \times 30$ mm behind a 9.6 mm thick Kevlar face sheet, modelled with C3D8R elements using a previously developed vectorised user material subroutine (VUMAT) [83]. A 9 mm full metal jacket (FMJ) bullet impacts the structure with an initial velocity of 358 m/s following the NIJ-STD-0106.01 standard. The FMJ, modelled with C3D8R elements, uses a Mie-Grüneisen hydrodynamic equation of state for the lead core and Johnson–Cook plasticity and damage for the brass outer

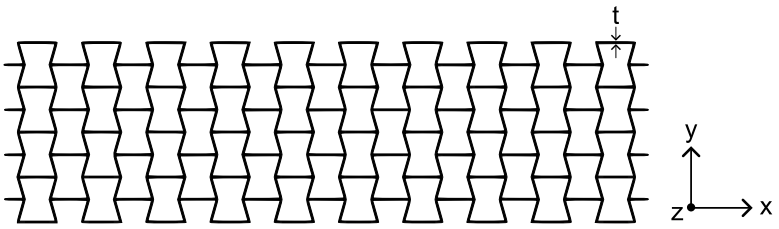

Fig. 1. 4 × 10 array of re-entrant cells for experimental impact with the wall thickness t.

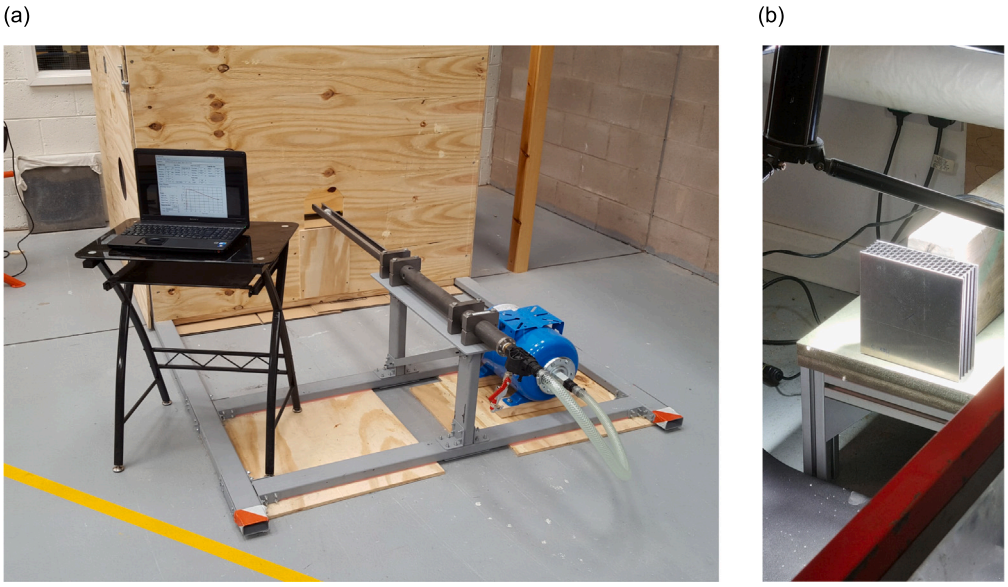

Fig. 2. Experimental impact set-up: (a) Simpact Engineering Ltd.'s Pneumatic Launcher - SPL 6000; (b) sample positioned for impact behind protective screens.

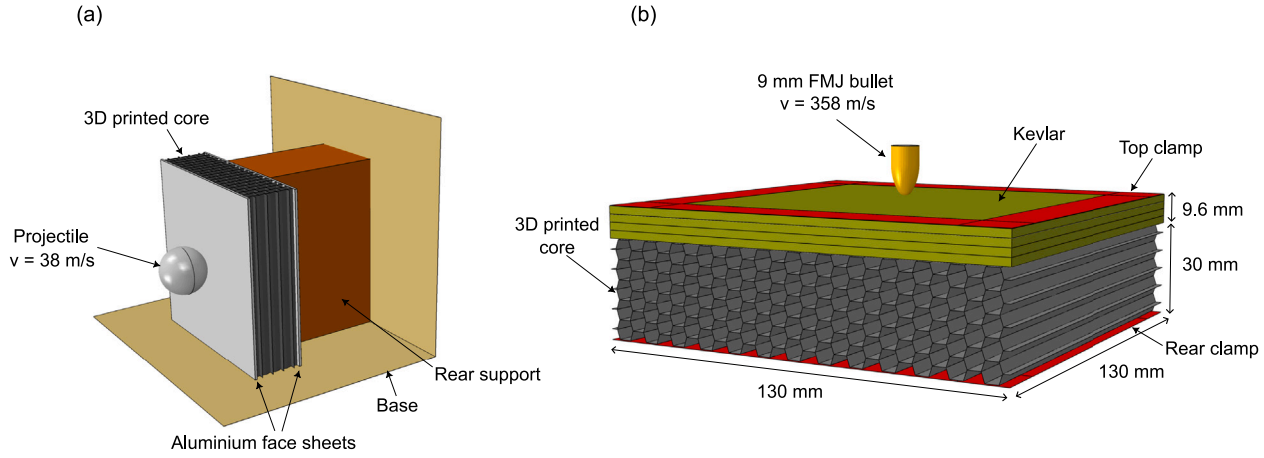

Fig. 3. Finite element models of (a) experimental impact setup with a projectile at 38 m/s impacting the 3D printed structure sat on a rigid base; (b) extended ballistic impact setup with a 9 mm FMJ bullet impacting a 3D printed structure with a Kevlar face sheet, clamped around the edge.

Table 1
Johnson–Cook material parameters for the 3D-printed core and aluminium face sheet.

Material	E (MPa)	A (MPa)	B (MPa)	n	C	$\dot{\epsilon}_0$ (1/s)	$r1$ (1/s)	$e1$	$r2$ (1/s)	$e2$	$r3$ (1/s)	$e3$
Onyx	1500	8.48	53.3	0.224	0.22	0.43	0.001	0.18	0.02	0.35	0.1	0.11
AA6082-T6	70000	305	304.9	0.67	0.0043	–	–	–	–	–	–	–

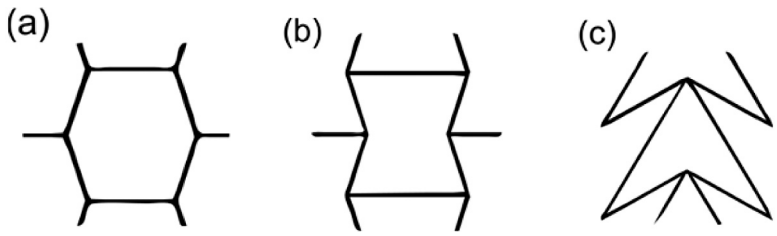

Fig. 4. Unit cells under investigation: (a) hexagonal, (b) re-entrant, (c) double arrowhead.

Table 2
Properties of aramid plate [84].

E_{11} (GPa)	E_{22}	E_{33}	G_{12}	G_{23}	G_{13}	ν_{12} –	ν_{13}	ν_{32}
18	18	4.5	0.77	2.6	2.6	0.25	0.33	0.33
X_{1t} (MPa)	X_{1c}	X_{2t}	X_{2c}	X_{3t}	X_{3c}	S_{12}	S_{13}	S_{23}
555	555	555	555	1050	1050	77	1060	1060

Table 3
Intralaminar fracture energies of aramid plate [83].

G_{ft} (N/mm^2)	G_{fc}	G_{mt}	G_{mc}
25	20	0.28	1.3

Table 4
Interlaminar damage parameters of aramid plate [84].

t_n (MPa)	t_s	t_t	G_n (N/mm^2)	G_s	G_t
34.5	9	9	0.24	0.47	0.47

Table 5
Mie-Grüneisen hydrodynamic equation of state parameters for lead core [84].

ρ (kg/m^3)	G (MPa)	c_0 (cm/μs)	s –	Γ_0 –	C_p (J kg^{-1} K^{-1})
11840	200	0.2006	1.429	2.6	150

Table 6
Johnson–Cook parameters for brass shell [84].

Plasticity	A	B	n	m	T_m(K)	T_{trans}(K)	C	ϵ_0(s^{-1})
	112	505	0.42	1.68	1189	373	0.009	1
Damage	d_1	d_2	d_3	d_4	d_5			
	0.54	4.89	3.03	0.0014	1.12			

shell. Material properties for the Kevlar, brass and lead are given in Tables 2–6 [83].

The structure is held in position by rigid clamps, fixed with an encastre boundary condition, that extend 15 mm from the edge of the specimen. During impact, the force transmitted to the clamps and the back face deformation (BFD) of the structure were monitored. Three unit cell geometries, Fig. 4, were considered: Hex, RE and DAH with the latter two being auxetic. The effect of relative density ($\overline{\rho}$), defined as the ratio of the density of the structure to the density of the base material, and unit cell size were also investigated.

3. Results & Discussion

This section presents the findings from both the experimental and numerical investigations of the 3D-printed auxetic re-entrant structure under high-velocity impact. The experimental results are first compared with the numerical simulations to validate the accuracy of the model, demonstrating a strong correlation between observed and predicted deformation and force transmission. Following this validation, the numerical analysis was extended to simulate ballistic impacts, allowing for the exploration of higher velocity conditions. Additionally, parametric studies were conducted to investigate the influence of varying relative density and cell size on the structure's performance. The results are discussed concerning existing literature, with an emphasis on their implications for the design of impact-resistant materials.

3.1. Experimental

Experimental testing of the 3D-printed auxetic re-entrant structure yielded data on force transmission and deformation under high-velocity impact. These results serve as a benchmark to validate the numerical model and to understand the structure's physical behaviour under impact conditions.

The numerical model predicted a permanent indent of 7.2 mm depth in the aluminium face sheet which is 4% greater than the experimental indent of 6.9 mm, measured using Mitutoyo digital callipers. The experimental and numerical deformation of the 3D-printed structure at maximum indentation is compared in Fig. 5. The auxetic nature of the structure is seen clearly, both on a cellular and a global level, where the folding of individual unit cells as well as an overall contraction of the structure is observed. Fig. 5 further confirms the understanding that auxetics densify under impact loading. The numerical deformation pattern is extremely similar to the experimental, exemplified by the close-up view in Fig. 5b. Failure of the adhesive between the face sheet and the outer cells, seen in Fig. 5a, was not captured by the numerical model due to the assumption of a perfect bond. This failure also reduced the global contraction seen in the experiment compared to the numerical prediction.

The experimental velocity profile of the steel ball was obtained by taking the derivative of its displacement, found using the motion tracking software. This was compared with the velocity extracted from the reference point of the rigid ball used in the numerical simulation in Fig. 6. Fluctuations are observed in the experimental velocity plot due to frame rate limitations of the high-speed camera. This is most significant at lower velocities, below ≈ 10 m/s, where the smaller distance between frames increased sensitivity to measurement noise, resulting in fluctuations in the derived velocity.

Overall, good agreement is observed between the numerical and experimental velocity–time curves with the ball reaching 0 m/s, corresponding to maximum displacement, at 0.95 and 1.05 ms respectively. The numerical simulation predicted a higher rebound velocity of 12 m/s compared to the experimentally recorded velocity of 7.6 m/s. This discrepancy can again be attributed to the assumption of a perfect bond in the numerical model. In the experimental impact, energy dissipated during the bond failure would reduce the kinetic energy of the ball and thus its rebound velocity. Slight rotation of the projectile was also observed during rebound which affected the accuracy of the motion tracking.

The strong correlation gives confidence in the material data and techniques used for modelling the 3D-printed cellular structures under impact loading, thus allowing for further numerical investigation into geometry and loading conditions.

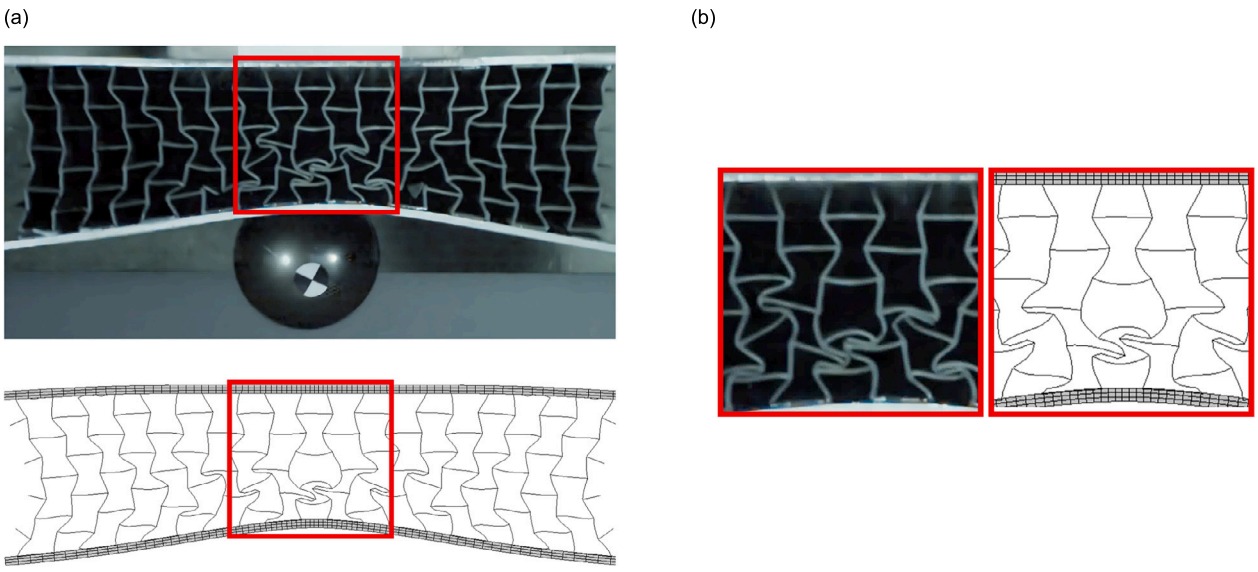

Fig. 5. Deformation of the 3D-printed structure under impact loading showing densification. (a) Global view: top — experimental, bottom — numerical; (b) Close-up view of central densified portion: left — experimental, right — numerical.

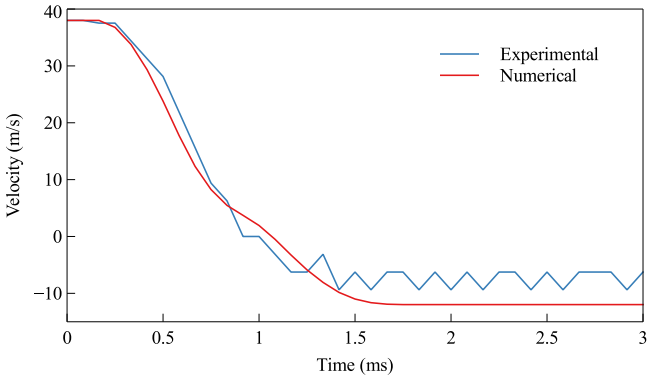

Fig. 6. Velocity–time graph of the steel ball during the impact event.

3.2. Parametric studies

The validated numerical model was further extended to simulate ballistic impacts as detailed in Section 2.2. Parametric studies were conducted to explore the influence of cell geometry, size and density on impact performance.

3.2.1. Cell geometry

Hexagonal, re-entrant and double arrowhead structures at a constant relative density were considered. Wall thicknesses of 0.84, 0.70 and 0.54 mm respectively were used to achieve a relative density of 30% for each structure.

The deformation of the three structures is shown in Fig. 7. The auxetic densification behaviour of the re-entrant and double arrowhead structures are clearly shown. The bending-dominated behaviour of the double arrowhead structure is observed, in contrast with the folding-dominated behaviour of the hexagonal and re-entrant. Bending of the cell walls, as opposed to folding/rotating around the nodes leads to reduced damage of the material. Numerical peak force and BFD data are tabulated in Table 7.

The force transferred to the rigid clamp was monitored and is shown in Fig. 8(a). The non-auxetic hexagonal structure transmitted a peak force of 25.7 kN, which is significantly higher than that of both auxetic structures. The re-entrant transmitted 18.8 kN, while the double arrowhead transmitted 14.3 kN, representing reductions of 27% and 44%, respectively, compared to the hexagonal structure. The duration of the force pulse was also notably greater for both of the auxetic structures. A lower, longer pulse such as this is typically correlated with less severe injury as the energy is dissipated over a longer time [85,86]. Increased BFD was observed in the auxetic structures, Fig. 8(b), in agreement with [87] who reported higher deformations in re-entrant structures compared with hexagonal under impact loading. The double arrowhead structure considered in this work underwent the greatest deformation, 17% higher than the hexagonal.

Table 7
Peak transmitted force and BFD for each geometry under consideration at 30% relative density.

Geometry	Hex	RE	DAH	RE → Hex	Hex → RE
Force (kN)	25.8	18.8	14.3	23.2	23.7
BFD (mm)	8.6	8.9	10.0	9.6	8.7

The Hex and RE structures share the same base geometry with differing oblique angles. As a result, it is possible to blend smoothly between the two unit cells, Fig. 9, creating a hybrid structure. A wall thickness of 0.77 mm, constant throughout the structure, results in an overall relative density of 30%, consistent with the previous analyses. The peak force transmitted during impact was similar for both orientations, close to the pure hexagonal structure. The BFD of each orientation, however, differed with the RE → Hex structure deforming approximately 10% more than the Hex → RE. This is a significant finding as it suggests the displacement response can be controlled independently of the force response, these results are included in Table 7. Applications such as body armour, helmets or protective structures often require minimal back face deformation whereas large deformations may be preferable in other applications such as seismic isolators.

3.2.2. Relative density

Three relative densities were considered: 20%, 30% and 40%, each obtained by varying the cell wall thickness, Table 8. A positive relation between relative density and transmitted force was observed across all unit cells, Fig. 10(a), whereas the BFD reduced with increasing relative density, Fig. 10(b). This is in agreement with Gibson & Ashby [1] who predict an increase in modulus with relative density, a result echoed experimentally by [88] who considered the out-of-plane compression of honeycomb structures.

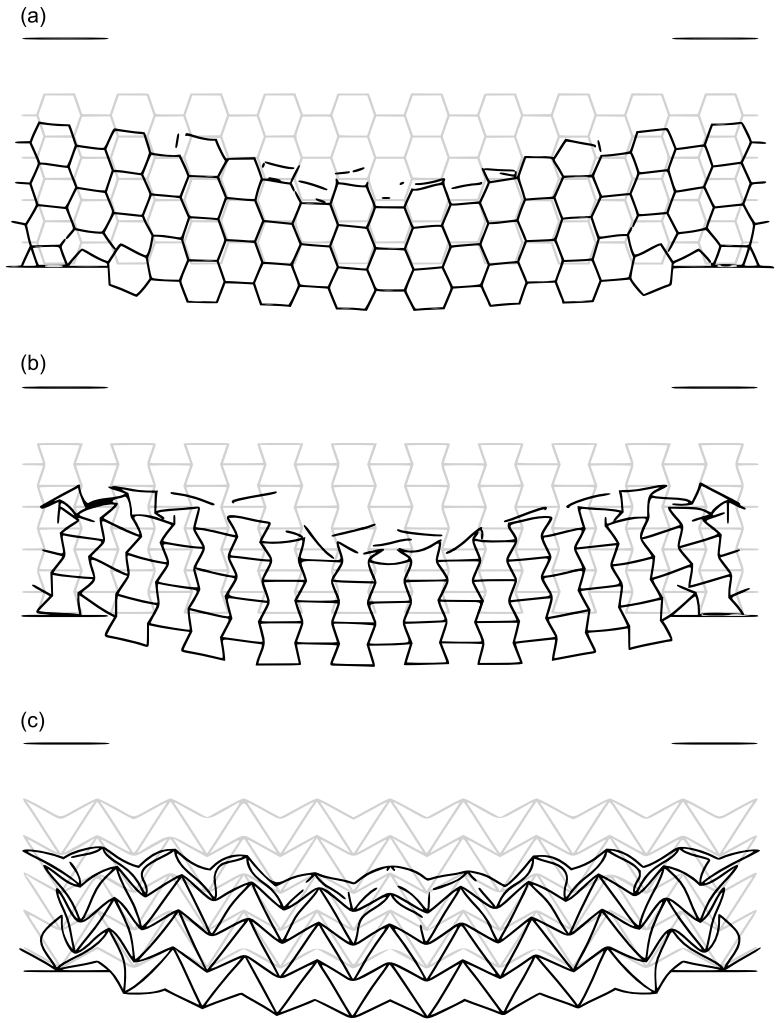

Fig. 7. Plots of the numerical deformation patterns: (a) hexagonal, (b) re-entrant, (c) double arrowhead. Undeformed shape in grey, deformed shape overlaid in black.

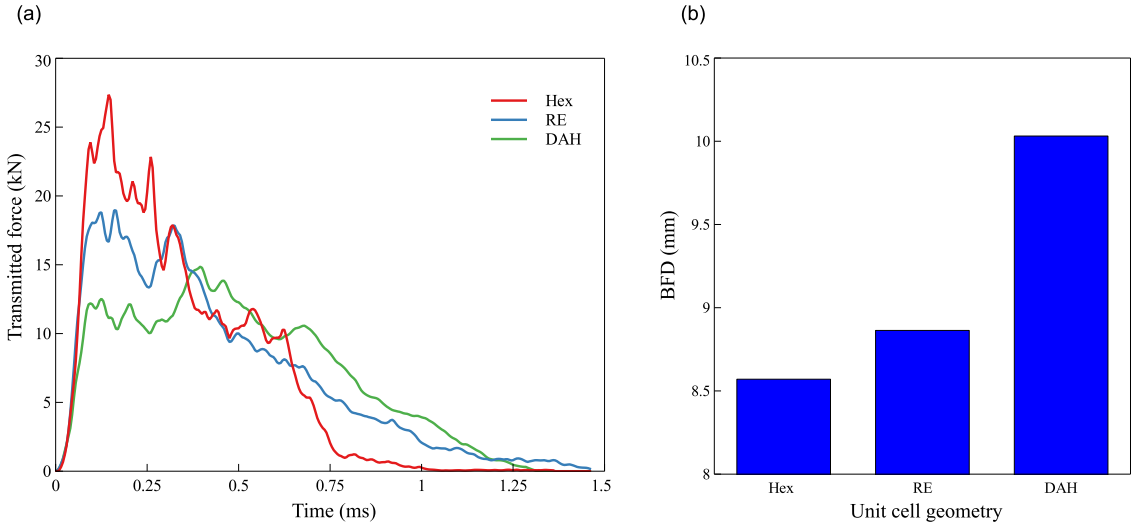

Fig. 8. Plot of (a) transmitted force and (b) back face deformation during impact for hexagonal, re-entrant and double arrowhead structures at 30% relative density.

3.2.3. Cell size

The effect of cell size on the impact response was explored by investigating five variants. The overall size of the structure was kept constant with the number of cells varied. Cells were arranged in 6 $\times 15, 5 \times 13, 4 \times 10, 3 \times 8$ and 2×5 arrays for extra-small (XS), small (S), medium (M), large (L) and extra-large (XL) respectively as shown in Fig. 11. The cell wall thicknesses were adjusted as per Table 9 to maintain a relative density of 30%.

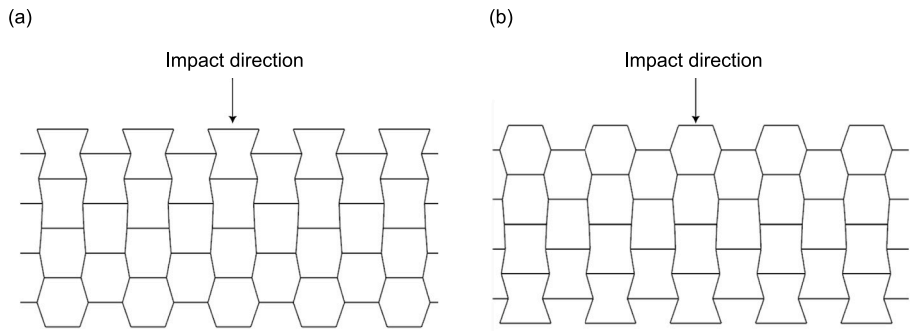

Fig. 9. Hybrid structure composing blended geometry in two orientations: (a) re-entrant → hexagonal, (b) hexagonal → re-entrant.

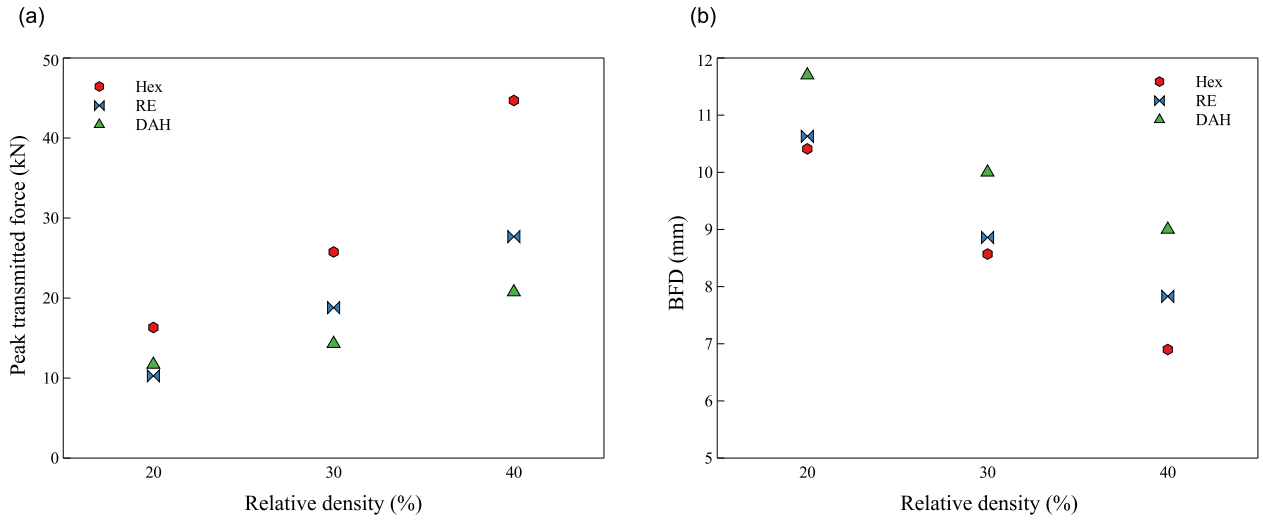

Fig. 10. Variation of (a) peak transmitted force and (b) BFD with relative density for the three structures.

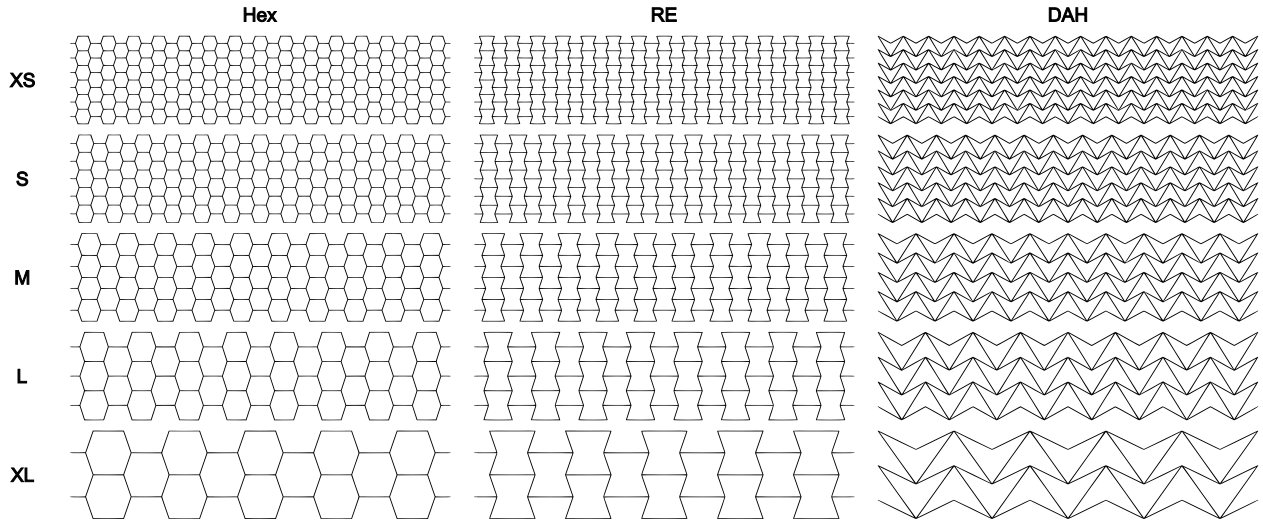

Fig. 11. Arrays of hexagonal (Hex), re-entrant (RE) and double arrowhead (DAH) unit cells in five sizes: extra-small (XS), small (S), medium (M), large (L) and extra-large (XL).

Fig. 12(a) shows a relatively consistent transmitted force until the medium cell size, after which the transmitted force begins to increase significantly. This can be attributed partially to the increase in wall thickness and partially to the concentration of force on a smaller number of struts at larger cell sizes. The increase is most significant for the hexagonal structure due to its bending-dominated deformation mechanism compared to the folding-dominated deformation of the auxetics. Supporting this, under ballistic impact Guo et al. [89] saw a reduction in residual velocity with increasing cell size for their re-entrant star honeycomb structure, indicating an increase in transmitted force.

Fig. 12(b) shows a non-linear relation between cell size and BFD, with the BFD increasing to a maximum before decreasing at larger sizes. Notably, the variation in deformation between geometries diminished with increasing cell size, indicating a reduced influence of cell geometry at larger sizes. These results suggest that for applications

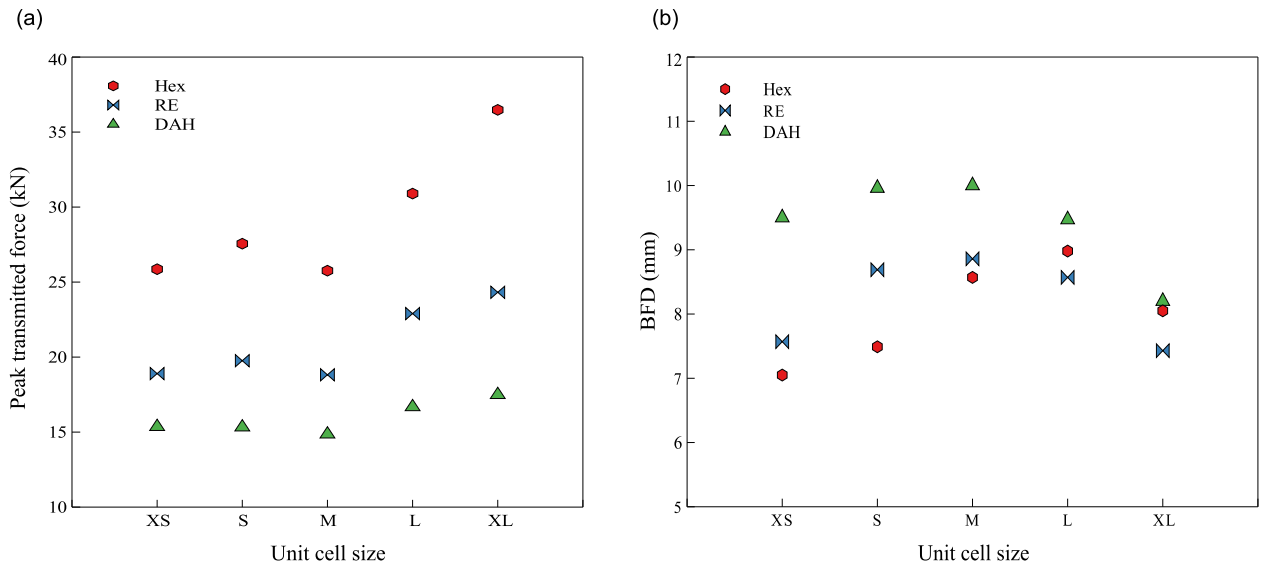

Fig. 12. Variation of (a) peak transmitted force and (b) BFD with unit cell size for the three structures.

Table 8
Cell wall thicknesses of 3D-printed structures for relative density investigations.

$\bar{\rho}$	Cell wall thickness (mm)		
(%)	20	30	40
Hex	0.71	0.84	1.41
RE	0.58	0.70	1.17
DAH	0.46	0.54	0.91

Table 9
Cell wall thicknesses of 3D-printed structures for unit cell size investigations.

	Cell wall thickness (mm)				
	XS	S	M	L	XL
Hex	0.72	0.84	1.07	1.35	2.03
RE	0.56	0.70	0.88	1.12	1.67
DAH	0.46	0.54	0.69	0.88	1.33

such as body armour or helmets, small structures may be optimal due to the minimisation of both transmitted force and BFD. If the force response is not critical, larger cell sizes can reduce BFD while enhancing manufacturability.

4. Conclusions

This study explored the impact response of 3D-printed mechanical metamaterials through experimental and numerical approaches. Experimentally, a 3D-printed re-entrant structure was impacted at 38 m/s. The auxetic behaviour was captured with high-speed footage clearly showing the densification characteristic of auxetic structures. The resultant indentation, deformation pattern and velocity–time response were closely replicated by a numerical model, validating the constitutive material model used.

The study extended these results by considering the response of these structures, with a Kevlar face sheet, under ballistic loading. Auxetic geometries, especially the double arrowhead, proved superior in force mitigation, reducing transmitted force by up to 44% compared to standard hexagonal structures of the same mass. Along with force mitigation, the auxetic structures increased the duration of the force pulse, a key factor in reducing injury. The potential of hybrid structures was also demonstrated, with a re-entrant to hexagonal transition offering a way to control deformation independently from force transmission. A hybrid structure with auxetic geometry on the impact face deformed 10% more than one with conventional geometry on the impact face, both transferring a similar peak force.

A parametric study showed an increase in transmitted force, along with a decrease in deformation, across all structures with increasing relative density. Complex relations were observed when investigating cell size effects. Transmitted force increased non-linearly with cell size, however, BFD peaked at a medium cell size, reducing for smaller and larger variants.

Although this study has provided new insights into the design of 3D-printed metamaterials for impact mitigation, there remain several areas for future work. Investigations into the effect of overall structure thickness would be beneficial, especially for space-limited applications such as body armour. Additionally, given the non-linearity of cell size effects, a potential relation between impactor size and cell size will be explored. Future studies will also explore the influence of other geometric parameters, such as cell wall angle, to fully optimise the mechanical properties of metamaterials for high-velocity impacts. Furthermore, different base materials should be investigated to assess their potential to enhance the impact resistance of these structures.

CRediT authorship contribution statement

Tom Fisher: Writing – review & editing, Writing – original draft, Visualization, Validation, Software, Methodology, Investigation, Formal analysis, Data curation, Conceptualization. **Zafer Kazancı:** Writing – review & editing, Supervision, Resources, Project administration, Funding acquisition. **José Humberto S. Almeida Jr.:** Writing – review & editing, Supervision, Resources, Project administration, Funding acquisition.

Declaration of competing interest

The authors declare that they have no known competing financial interests or personal relationships that could have appeared to influence the work reported in this paper.

Acknowledgements

This research was kindly funded by an EPSRC Standard Research Studentship (2442948). The authors are extremely grateful for Simpact Engineering Ltd.'s support in carrying out the experimental testing.

Data availability

Data will be made available on request.

References

[1] Gibson LJ, Ashby MF. Cellular solids: structure and properties. 2nd ed.. 1997.
[2] Schaedler TA, Carter WB. Architected cellular materials. Annu Rev Mater Res 2016;46:187–210.
[3] Uribe-Lam E, Treviño-Quintanilla CD, Cuan-Urquizo E, Olvera-Silva O. Use of additive manufacturing for the fabrication of cellular and lattice materials: a review. Mater Manuf Process 2021;36(3):257–80.
[4] Zhou X, Ren L, Song Z, Li G, Zhang J, Li B, Wu Q, Li W, Ren L, Liu Q. Advances in 3D/4D printing of mechanical metamaterials: From manufacturing to applications. Composites B 2023;254:110585.
[5] Jiang W, Yin G, Xie L, Yin M. Multifunctional 3D lattice metamaterials for vibration mitigation and energy absorption. Int J Mech Sci 2022;233:107678.
[6] Ashby MF, Gibson LJ. Cellular solids: Structure & properties. Permagon Press; 1988.
[7] Andrew JJ, Ubaid J, Hafeez F, Schiffer A, Kumar S. Impact performance enhancement of honeycombs through additive manufacturing-enabled geometrical tailoring. Int J Impact Eng 2019;134:103360.
[8] Christoff BG, Almeida JHS, Cardoso EL, Tita V. A multiscale topology optimisation framework for hollow spheres as cellular materials. Eng Struct 2023;284:115990.
[9] Montazeri A, Naderinejad M, Mahnama M, Hasani A. 3D-printed twisting tubular metamaterials with tunable mechanical and torsional characteristics. Int J Mech Sci 2024;262:108719.
[10] Valizadeh I, Weeger O. Parametric visco-hyperelastic constitutive modeling of functionally graded 3D printed polymers. Int J Mech Sci 2022;226:107335.
[11] Kang JH, Sakthiabirami K, Jang KJ, Jang JG, Oh GJ, Park C, Fisher JG, Park SW. Mechanical and biological evaluation of lattice structured hydroxyapatite scaffolds produced via stereolithography additive manufacturing. Mater Des 2022;214:110372.
[12] Bouteldja A, Louar MA, Hemmouche L, Gilson L, Miranda-Vicario A, Rabet L. Experimental investigation of the quasi-static and dynamic compressive behavior of polymer-based 3D-printed lattice structures. Int J Impact Eng 2023;180:104640.
[13] Cuan-Urquizo E, Guerra Silva R. Fused filament fabrication of cellular, lattice and porous mechanical metamaterials: a review. Virtual Phys Prototyp 2023;18(1).
[14] Gautam R, Idapalapati S, Feih S. Printing and characterisation of Kagome lattice structures by fused deposition modelling. Mater Des 2018;137:266–75.
[15] Bodaghi M, Damanpack AR, Liao WH. Adaptive metamaterials by functionally graded 4D printing. Mater Des 2017;135:26–36.
[16] Almeida JHS, Christoff BG, Tita V, St-Pierre L. A concurrent fibre orientation and topology optimisation framework for 3D-printed fibre-reinforced composites. Compos Sci Technol 2023;232:109872.
[17] Harris JA, Winter RE, McShane GJ. Impact response of additively manufactured metallic hybrid lattice materials. Int J Impact Eng 2017;104:177–91.
[18] Ramos H, Santiago R, Soe S, Theobald P, Alves M. Response of gyroid lattice structures to impact loads. Int J Impact Eng 2022;164:104202.
[19] Al-Saedi DS, Masood SH, Faizan-Ur-Rab M, Alomarah A, Ponnusamy P. Mechanical properties and energy absorption capability of functionally graded F2BCC lattice fabricated by SLM. Mater Des 2018;144:32–44.
[20] Leary M, Mazur M, Williams H, Yang E, Alghamdi A, Lozanovski B, Zhang X, Shidid D, Farahbod-Sternahl L, Witt G, Kelbassa I, Choong P, Qian M, Brandt M. Inconel 625 lattice structures manufactured by selective laser melting (SLM): Mechanical properties, deformation and failure modes. Mater Des 2018;157:179–99.
[21] Isaac CW, Duddeck F. Current trends in additively manufactured (3D printed) energy absorbing structures for crashworthiness application – a review. Virtual Phys Prototyp 2022;17(4):1058–101.
[22] Simpson J, Kazancı Z. Crushing investigation of crash boxes filled with honeycomb and re-entrant (auxetic) lattices. Thin-Walled Struct 2020;150:106676.
[23] Guo W, Yang L, Xu P, Li S, Yan W, Shen Z, Yao S, Yang C. Crashworthiness analysis of okra biomimetic corrugated multi-cellular structure. Int J Mech Sci 2024;280:109459.
[24] Xu P, Guo W, Yang L, Yang C, Ruan D, Xu J, Yao S. Crashworthiness analysis of the biomimetic lotus root lattice structure. Int J Mech Sci 2024;263:108774.
[25] Hou W, He P, Yang Y, Sang L. Crashworthiness optimization of crash box with 3D-printed lattice structures. Int J Mech Sci 2023;247:108198.
[26] Wei Y, Zhang C, Yuan Y, Chen P, Huang C, Li J, Yuan M. Blast response of additive manufactured Ti–6Al–4V sandwich panels. Int J Impact Eng 2023;176:104553.
[27] Kamel H. Review of design techniques of armored vehicles for protection against blast from improvised explosive devices. In: ASME international mechanical engineering congress and exposition, proceedings (IMECE). vol. 13, American Society of Mechanical Engineers Digital Collection; 2020.
[28] Imbalzano G, Linforth S, Ngo TD, Lee PVS, Tran P. Blast resistance of auxetic and honeycomb sandwich panels: Comparisons and parametric designs. Compos Struct 2018;183(1):242–61.
[29] Qi C, Remennikov A, Pei LZ, Yang S, Yu ZH, Ngo TD. Impact and close-in blast response of auxetic honeycomb-cored sandwich panels: Experimental tests and numerical simulations. Compos Struct 2017;180:161–78.
[30] Zhang J, Lu G, You Z. Large deformation and energy absorption of additively manufactured auxetic materials and structures: A review. Composites B 2020;201:108340.
[31] Bohara RP, Linforth S, Nguyen T, Ghazlan A, Ngo T. Novel lightweight high-energy absorbing auxetic structures guided by topology optimisation. Int J Mech Sci 2021;211:106793.
[32] Shokri Rad M, Hatami H, Alipouri R, Farokhi Nejad A, Omidinasab F. Determination of energy absorption in different cellular auxetic structures. Mech Ind 2019;20(3):302.
[33] Gao Q, Liao W-H. Energy absorption of thin walled tube filled with gradient auxetic structures-theory and simulation. Int J Mech Sci 2021;201:106475.
[34] Linforth S, Ngo T, Tran P, Ruan D, Odish R. Investigation of the auxetic oval structure for energy absorption through quasi-static and dynamic experiments. Int J Impact Eng 2021;147:103741.
[35] Etemadi E, Hosseinabadi M, Taghizadeh M, Scarpa F, Hu H. Enhancing the energy absorption capability of auxetic metamaterials through auxetic cells within re-entrant circular units. Eng Struct 2024;315:118379.
[36] Zhang C, Lu F, Wei T, Huang Y, He Y, Zhu Y. A novel windmill-shaped auxetic structure with energy absorption enhancement. Int J Mech Sci 2024;280:109635.
[37] Novak N, Vesenjak M, Tanaka S, Hokamoto K, Ren Z. Compressive behaviour of chiral auxetic cellular structures at different strain rates. Int J Impact Eng 2020;141:103566.
[38] Najafi M, Ahmadi H, Liaghat G. Experimental investigation on energy absorption of auxetic structures. Mater Today: Proc 2020.
[39] Qi C, Yang S, Wang D, Yang LJ. Ballistic resistance of honeycomb sandwich panels under in-plane high-velocity impact. Sci World J 2013;2013.
[40] Mohamed RA, Lawaty SM, El-Butch AM. Ballistic impact response of an aluminum sandwich panel with auxetic honeycomb core structure. In: Proceedings of the 17th int. AMME conference. 2016, p. 16–27.
[41] Madke RR, Chowdhury R. Anti-impact behavior of auxetic sandwich structure with braided face sheets and 3D re-entrant cores. Compos Struct 2020;236.
[42] Critchley R, Hazael R, Bhatti K, Wood D, Peare A, Johnson S, Temple T. Blast mitigation using polymeric 3D printed auxetic re-entrant honeycomb structures: A preliminary study. Int J Prot Struct 2022;13(3):469–86.
[43] Bohara RP, Linforth S, Nguyen T, Ghazlan A, Ngo T. Anti-blast and -impact performances of auxetic structures: A review of structures, materials, methods, and fabrications. Eng Struct 2023;276:115377.
[44] Jiang F, Yang S, Qi C, Liu HT, Remennikov A, Pei LZ. Blast response and multi-objective optimization of graded re-entrant circular auxetic cored sandwich panels. Compos Struct 2023;305:116494.
[45] Wang G, Deng X. In-plane mechanical behavior design of novel re-entrant and hexagonal combined honeycombs. Mater Today Commun 2024;40:109729.
[46] Zou Z, Xu F, Niu X, Xie C, Fang T. In-plane crashing behavior and energy absorption of graded re-entrant honeycombs reinforced by catenary. Thin-Walled Struct 2024;203:112253.
[47] Guo MF, Yang H, Ma L. Design and characterization of 3D AuxHex lattice structures. Int J Mech Sci 2020;181:105700.
[48] Tan H, He Z, Li E, Tan X, Cheng A, Li Q. Energy absorption characteristics of three-layered sandwich panels with graded re-entrant hierarchical honeycombs cores. Aerosp Sci Technol 2020;106:106073.
[49] Li Z, Gao Q, Yang S, Wang L, Tang J. Comparative study of the in-plane uniaxial and biaxial crushing of hexagonal, re-entrant, and mixed honeycombs. J Sandw Struct Mater 2019;21(6):1991–2013.
[50] Ingrole A, Hao A, Liang R. Design and modeling of auxetic and hybrid honeycomb structures for in-plane property enhancement. Mater Des 2017;117:72–83.
[51] Bagewadi SS, Sugavaneswaran M, Bhagchandani RK. Investigation on mechanical properties of additive manufactured hybrid auxetic structure. J Mater Eng Perform 2023;32(1):68–81.
[52] Nian Y, Wan S, Avcar M, Yue R, Li M. 3D printing functionally graded metamaterial structure: Design, fabrication, reinforcement, optimization. Int J Mech Sci 2023;258:108580.
[53] Qiao JX, Chen CQ. Impact resistance of uniform and functionally graded auxetic double arrowhead honeycombs. Int J Impact Eng 2015;83:47–58.
[54] Tomita S, Shimanuki K, Umemoto K. Control of buckling behavior in origami-based auxetic structures by functionally graded thickness. J Appl Phys 2024;135(10).
[55] Hou Y, Tai YH, Lira C, Scarpa F, Yates JR, Gu B. The bending and failure of sandwich structures with auxetic gradient cellular cores. Composites A 2013;49:119–31.
[56] Boldrin L, Hummel S, Scarpa F, Di Maio D, Lira C, Ruzzene M, Remillat CD, Lim TC, Rajasekaran R, Patsias S. Dynamic behaviour of auxetic gradient composite hexagonal honeycombs. Compos Struct 2016;149:114–24.

[57] Zhang J, Dong B, Zhang W. Dynamic crushing of gradient auxetic honeycombs. J Vib Eng Technol 2021;9(3):421–31.
[58] Lira C, Scarpa F, Rajasekaran R. a gradient cellular core for aeroengine fan blades based on auxetic configurations. J Intell Mater Syst Struct 2011;22(9):907–17.
[59] Nur Ainin F, Azaman MD, Abdul Majid MS, Ridzuan MJ. Low-velocity impact behavior of sandwich composite structure with 3D printed hexagonal honeycomb core: varying core materials. Funct Compos Struct 2022;4(3):035007.
[60] Nur Ainin F, Azaman MD, Abdul Majid MS, Ridzuan MJ. Investigating the low-velocity impact behaviour of sandwich composite structures with 3D-printed hexagonal honeycomb core—a review. Funct Compos Struct 2023;5(1):012001.
[61] Li Z, Wang T, Jiang Y, Wang L, Liu D. Design-oriented crushing analysis of hexagonal honeycomb core under in-plane compression. Compos Struct 2018;187:429–38.
[62] Liu W, Wang N, Luo T, Lin Z. In-plane dynamic crushing of re-entrant auxetic cellular structure. Mater Des 2016;100:84–91.
[63] Usta F, Türkmen HS, Scarpa F. High-velocity impact resistance of doubly curved sandwich panels with re-entrant honeycomb and foam core. Int J Impact Eng 2022;165:104230.
[64] Kumar S, Vyavahare S, Bogala H. Double arrowhead auxetic structures: A numerical investigation under compressive loading. Lect Not Mech Eng 2022;35–50.
[65] Wang XT, Wang B, Wen ZH, Ma L. Fabrication and mechanical properties of CFRP composite three-dimensional double-arrow-head auxetic structures. Compos Sci Technol 2018;164:92–102.
[66] Gu L, Xu Q, Zheng D, Zou H, Liu Z, Du Z. Analysis of the mechanical properties of double arrowhead auxetic metamaterials under tension. Text Res J 2020;90(21–22):2411–27.
[67] Martín MJ, Auñón JA, Martín F. Influence of infill pattern on mechanical behavior of polymeric and composites specimens manufactured using fused filament fabrication technology. Polymers 2021, Vol. 13, Page 2934 2021;13(17):2934.
[68] Blok LG, Longana ML, Yu H, Woods BK. An investigation into 3D printing of fibre reinforced thermoplastic composites. Addit Manuf 2018;22:176–86.
[69] Almeida Jr JHS, Miettinen A, Léonard F, Falzon BG, Withers PJ. Microstructure and damage evolution in short carbon fibre 3D-printed composites during tensile straining. Composites Part B: Engineering 2025;292:112073.
[70] Fisher T, Almeida Jr JHS, Falzon BG, Kazancı Z. Tension and compression properties of 3D-printed composites: Print orientation and strain rate effects. Polymers 2023;15(7):1708.
[71] Fisher T, Kazancı Z, Almeida Jr H. The importance of print orientation in numerical modelling of 3D printed structures under impact loading. Mater Res Express 2024.
[72] Chen Y, Ye L, Zhang YX, Fu K. Compression behaviours of 3D-printed CF/PA metamaterials: Experiment and modelling. Int J Mech Sci 2021;206:106634.
[73] Yang K, Li Z, Huang P, Lin Y, Huang L. Mechanical and failure characteristics of novel tailorable architected metamaterials against crash impact. Eng Fail Anal 2024;159:108141.
[74] Alomarah A, Yuan Y, Ruan D. A bio-inspired auxetic metamaterial with two plateau regimes: Compressive properties and energy absorption. Thin-Walled Struct 2023;192:111175.
[75] Xu Mm, Huang Gy, Feng Ss, Qin Xy, McShane GJ, Stronge WJ. Perforation resistance of aluminum/polyethylene sandwich structure. Mater Des 2016;100:92–101.
[76] Günaydın K, Rea C, Kazancı Z. Energy absorption enhancement of additively manufactured hexagonal and re-entrant (auxetic) lattice structures by using multi-material reinforcements. Addit Manuf 2022;59:103076.
[77] Wu C, Peng C, Le TC, Das R, Tran P. Tunable 3D printed composite metamaterials with negative stiffness. Smart Mater Struct 2023;32(12):125010.
[78] Sukia I, Morales U, Esnaola A, Aurrekoetxea J, Erice B. Low-velocity impact performance of integrally-3D printed continuous carbon fibre composite sandwich panels. Mater Lett 2024;354:135374.
[79] Chen W, Hudspeth M, Guo Z, Lim BH, Horner S, Zheng JQ. Multi-scale experiments on soft body armors under projectile normal impact. Int J Impact Eng 2017;108:63–72.
[80] Nair AN, Sundharesan S, Al Tubi ISM. Kevlar-based composite material and its applications in body armour: A short literature review. IOP Conf Ser: Mater Sci Eng 2020;987(1):012003.
[81] Palta E, Fang H, Weggel DC. Finite element analysis of the advanced combat helmet under various ballistic impacts. Int J Impact Eng 2018;112:125–43.
[82] Rodriguez-Millan M, Rubio I, Burpo FJ, Tse KM, Olmedo A, Loya JA, Parker KK, Miguélez MH. Experimental and numerical analyses of ballistic resistance evaluation of combat helmet using hybrid III headform. Int J Impact Eng 2023;179:104653.
[83] Fisher T, Almeida Jr JHS, Burhan M, Kazancı Z. Development of a new progressive damage model for woven fabric composites. Mech Adv Mater Struct 2024;1–7.
[84] MING TK. Development of a realistic finite element model of human head and its applications to head injuries [Ph.D. thesis], National University of Singapore; 2013.
[85] Bartlett R. Introduction to sports biomechanics : analysing human movement patterns. 2007, p. 292.
[86] Saboori P, Walker G. Brain injury and impact characteristics. Ann Biomed Eng 2019;47(9):1982–92.
[87] Yazdani Sarvestani H, Akbarzadeh AH, Niknam H, Hermenean K. 3D printed architected polymeric sandwich panels: Energy absorption and structural performance. Compos Struct 2018;200:886–909.
[88] Zhou J, Ng BF, Han N, Xu S, Zou M. Crashworthiness and optimization of bionic sandwich cores under out-of-plane compression. Int J Mech Sci 2023;246:108137.
[89] Guo J, He Q, Li L, Zhu J, Yan D. Ballistic resistance of a novel re-entrant auxetic honeycomb under in-plane high-velocity impact. J Compos Mater 2024;58(8):1031–49.